

Social stress drives the multi-wave dynamics of COVID-19 outbreaks

Innokentiy A. Kastalskiy^{1,2,3,*}, Evgeniya V. Pankratova⁴, Evgeny M. Mirkes^{5,6},

Victor B. Kazantsev^{1,3,7,8} & Alexander N. Gorban^{1,5,6}

¹Department of Neurotechnology, Lobachevsky University, 23 Gagarin Ave., 603022 Nizhny Novgorod, Russia

²Laboratory of Autowave Processes, Institute of Applied Physics of the Russian Academy of Sciences (IAP RAS), 46 Ul'yanov Str., 603950 Nizhny Novgorod, Russia

³Center for Neurotechnology and Machine Learning, Immanuel Kant Baltic Federal University, 14 Nevsky Str., 236016 Kaliningrad, Russia

⁴Department of Applied Mathematics, Institute of Information Technology, Mathematics and Mechanics, Lobachevsky University, 23 Gagarin Ave., 603022 Nizhny Novgorod, Russia

⁵Laboratory of Perspective Methods for Analysis of Multidimensional Data, Institute of Information Technology, Mathematics and Mechanics, Lobachevsky University, 23 Gagarin Ave., 603022 Nizhny Novgorod, Russia

⁶Department of Mathematics, University of Leicester, University Rd, Leicester LE1 7RH, United Kingdom

⁷Neuroscience and Cognitive Technology Laboratory, Innopolis University, 1 Universitetskaya Str., 420500 Innopolis, Russia

⁸Laboratory of Neuromodeling, Samara State Medical University, 18 Gagarin Str., 443079 Samara, Russia

*email: kastalskiy@neuro.nnov.ru

Abstract

The dynamics of epidemics depend on how people's behavior changes during an outbreak. The impact of this effect due to control interventions on the morbidity rate is obvious and supported by numerous studies based on SIR-type models¹⁻⁶. However, the existing models do not explain the difference in outbreak profiles in countries with different intrinsic socio-cultural features and are rather specific for describing the complex dynamics of an outbreak. A system of models of the COVID-19 pandemic is proposed, combining the dynamics of social stress⁷ described by the tools of sociophysics⁸ with classical epidemic models. Even the combination of a dynamic SIR model with the classic triad of stages of general adaptation syndrome⁷, Alarm-Resistance-Exhaustion, makes it possible to describe the available statistics for various countries of the world with a high degree of accuracy. The conceptualization of social stress leads to the division of the vulnerable population into different groups according to behavior mode, which can be tracked in detail. The sets of kinetic constants corresponding to optimal fit of model to data clearly characterize the society ability to focus efforts on protection against pandemic and keep this concentration for a considerable time. Such characterization can further help in the development of management strategies specific to a particular society: country, region, or social group.

Introduction

In December 2019, the growing number of severe cases of pneumonia was reported in Wuhan city, Hubei Province, People's Republic of China. Strong infectivity of the virus led to the spread of an infectious disease all over the world in about three months. Therefore, on March 11, 2020, the World Health Organization declared a global pandemic. Causing potentially fatal respiratory syndrome, a novel type of coronavirus, nowadays known as severe acute respiratory syndrome coronavirus 2 (SARS-CoV-2), led to tremendous changes in economy, education and our daily life.

From the beginning of the pandemic, a lot of mathematical models have been proposed to simulate the virus spread and possible ways of its control. Assuming that population is mixed

homogeneously it is possible to describe qualitatively the infection outbreak using SIR-type models and their modifications. In particular, various SEIR-type^{2,9,10} (susceptible-exposed-infected-removed), SEIQR-type⁴ (additional quarantined), SEIR models with delays^{5,11,12}, SIR-type time-dependent¹³ and compartmental models¹⁴, or even SEIIHURD model¹⁵ with the proportion of symptomatic needing hospitalization and those in critical conditions requiring intensive care admission, and many others accounting different particular factors have been proposed. Specifically, various complicated high-dimensional social network models can be considered. For example, the one of the heterogeneous SAIR-models¹⁶ (susceptible-asymptomatic-infected-removed), allows taking into account various numbers of contacts between individuals in the network as various degrees of the network nodes.

Taking into account recent data, emergence of the second and consequent peaks in the epidemic dynamics and effective ways of their control have become of particular interest. In recent work¹⁷, to analyze the ways to reduce the rate of SARS-CoV-2 virus transmission, eight-dimensional SEIR-type model was proposed. Based on its analysis the double-peak behavior caused by removing restrictions was demonstrated³. It was also shown that the second peak could be even much higher than the first one.

It has become obvious that in modern world cobweb-shrouded by TV, internet, and social networks providing instantaneous information transfer social factors should significantly influence on the population response to the epidemic stress intervention. Various stress factors can significantly modify social dynamics⁸ as well as information spreading in time of crisis¹⁸. Necessity to change the usual way of people's life (fear of dire consequences for the health, administrative restrictions and so on) leads to a significant change in the effective reproduction number. In recent research⁶, the entire population was divided into the groups where the persons either obey the social distancing rules or disregard them. Such assumption found the social factors-dependent size of these groups, and expectedly reveals an oscillating mode of repeated relaxations (when it seems that the situation is improved) and tightening of restrictions (when infection spreading becomes high).

General Adaptation Syndrome (GAS) was discovered by Selye (1936)¹⁹. He found that “a typical syndrome appears, the symptoms of which are independent of the nature of the damaging agent”. Later on, this concept was integrated with Cannon’s *fight-or-flight response*²⁰, and the general concept of stress was developed with a wide range of applications in physiology, psychology and beyond²¹⁻²³.

GAS consists of three phases: a mobilization phase, *Alarm*, a *Resistance* phase, and an *Exhaustion* phase⁷. To simulate the population dynamics within the conditions of aggressive COVID-19 spreading, the susceptible group of the persons can be divided into three subgroups of the individuals including (i) *ignorant* mode (persons living without any restrictions as it was before the pandemic), (ii) *resistance* mode (conscious persons practicing the social *distancing* rules to avoid the appeared danger) and (iii) *exhaustion* mode (the depletion of the person's resources leading to reduction of following social distancing rules). In the first approximation, we exclude the *alarm* mode that may be considered as a short delay before activation of resistant behavior. In more detailed models, alarm mode can be considered separately, but the more phases we consider, the more unknown constants we have to identify, and the simplest model should be tested first.

Incorporating the social stress in our SIR-type model (SIR_{ss}) immediately shows the multi-peak dynamics in the COVID-19 outbreaks. The model parameters have been successfully fitted to best match the statistical observations of epidemics in different countries of the world.

The parameters of social dynamics found for different countries demonstrate the differences between their social reactions to pandemic stress. The qualitative picture meets the general expectations, but the quantitative differences between countries are instructive and can be used in the development of management strategies specific to a particular society: country, region, or social group because the modeling method can be directly transferred and applied to regions, cities, and big enough subpopulations.

Results

Adjustment of the SIR_{ss} model parameters. Monitoring the global epidemiological situation and assessments based on trivial SIR models show that the first epidemic wave decays more rapidly than the models prescribe, and then a second wave observed in the empirical data but not in SIR model emerges. The premature decline in the morbidity rate can be attributed to social stress factor and the emergence of cautious behavior.

We propose SIR_{ss} mathematical model taking into account social stress factor as an intrinsic response of the humans to an external stimulus. Dividing susceptible people into three subgroups depending on behavior mode has significantly enriched the number of transitions between fractions and the dimension of the SIR model. Thus, the model describes dynamics of five groups:

Susceptible individuals (S) split in three subgroups by the types of behavior: *ignorant* or unaware of the epidemic (S_{ign}), rationally *resistant* (S_{res}), and *exhausted*, neglecting protection (S_{exh}). In other words: $S = S_{ign} + S_{res} + S_{exh}$. Two other groups are *infected* person (I) and *recovered* (R).

Let us employ the standard in sociophysics quasichemical representation of processes. SIR models is presented by two types of transitions: $S + I \rightarrow 2I$ and $I \rightarrow R$. For the extended model, the first transition transforms into $S_{exh} + I \rightarrow 2I$ and $S_{ign} + I \rightarrow 2I$ with the same parameters as in the basic SIR model. The additional sociophysical transitions are (1) $S_{ign} + 2I \rightarrow S_{res} + 2I$ – mobilization reaction, (2) $S_{res} \rightarrow S_{exh}$ – exhaustion due to restrictions; (3) $S_{exh} \rightarrow S_{ign}$ – relaxation to initial state (end of refractory period). In more detail, the model is described in Section “Methods”.

We kept fixed following parameters: $b = 0.1$ (recovery rate $I \rightarrow R$, expected period of being infected is $b^{-1} = 10$ days), $K_3 = 0.01$ ($S_{exh} \rightarrow S_{ign}$, expected period of being exhausted is $K_3^{-1} = 100$ days). The other parameters a (morbidity rate, $S + I \rightarrow 2I$), K_2 (exhaustion rate, $S_{res} \rightarrow S_{exh}$), and q (stress response rate, $S_{ign} + 2I \rightarrow S_{res} + 2I$) were varied to fit experimental data. An additional parameter that affects the rate of the outbreak and, hence, the time of the first wave maximum, was $I_0 = I(t=0)$, e.g. the initial fraction of infected people in the population.

We used simulations to fit the cumulative cases observations (CC) in China and in general sample containing 12 countries, mainly from the top-10 in terms of the number of coronavirus cases: Brazil, Colombia, France, Germany, India, Iran, Israel, Italy, Russia, Spain, UK, and USA. We took a simulation duration that fully comprises the first epidemic wave, but not too long to be influenced of seasonal fluctuations in immunity. An interval of 200 days was chosen as the priority period for simulations. We used the calculation of R^2 coefficient as goodness of fit measure to perform global optimization in the parameter space (a, K_2, q, I_0). Finally, we have identified the precise values of these parameters, which provide the best fit between the theoretical curve $CC(t)$ and the observed one. The results are shown in **Table 1**.

Table 1 Key epidemiological parameters used in simulations to explain the COVID-19 observations

Country or territory	Population	Number of days modeled	Parameters				R^2
			a	$K_2 \times 10^{-3}$	$q \times 10^3$	$I_0 \times 10^{-6}$	
China	1,439,324 K	200	0.2902	2.67	378370	1.00	0.99460
Brazil	212,559 K	300	0.1371	15.36	3.21	36.6	0.99911
Colombia	50,883 K	300	0.1451	20.84	5.84	5.72	0.99971
France	68,148 K	200	0.3138	5.43	213.5	0.36*	0.98727
Germany	83,784 K	200	0.2190	6.06	292.7	18.0	0.99898
India	1,380,004 K	400	0.1346	6.76	27.0	2.64	0.99730
Iran	83,993 K	100	0.2096	20.36	1322	11.5	0.99910
Israel	8,656 K	100	0.2473	7.85	397.8	34.8	0.99311
Italy	60,462 K	200	0.1929	5.22	87.1	38.4	0.99713
Russia	145,934 K	200	0.1495	13.45	47.5	35.9	0.99878
Spain	46,755 K	200	0.3770	4.56	75.4	1.17*	0.98844
UK	67,886 K	200	0.1798	7.27	83.7	28.5	0.99828
USA	331,003 K	150	0.2065	19.23	85.2	19.2	0.99899
Median	83,784 K	200	0.2065	7.27	85.2	18.0	0.99828

*Unusually small I_0 for France and Spain may be caused by numerous data corrections in April'20-May'20

Notice that in China, the resistance index q is unprecedentedly higher than in other densely populated countries. It immediately indicates that the highest discipline and government control that we observed in China permits to avoid the second wave of coronavirus outbreak (**Fig. 1**).

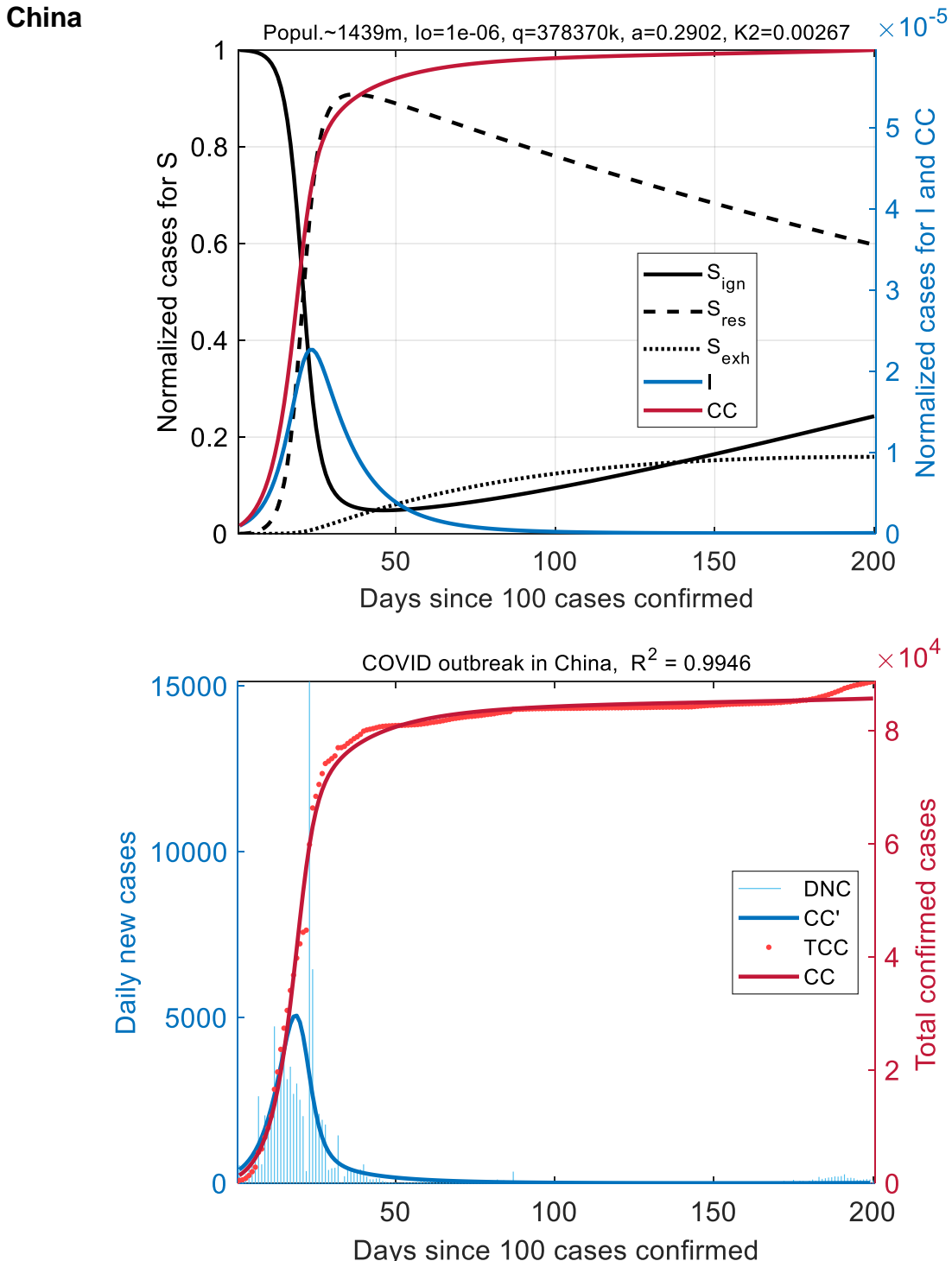
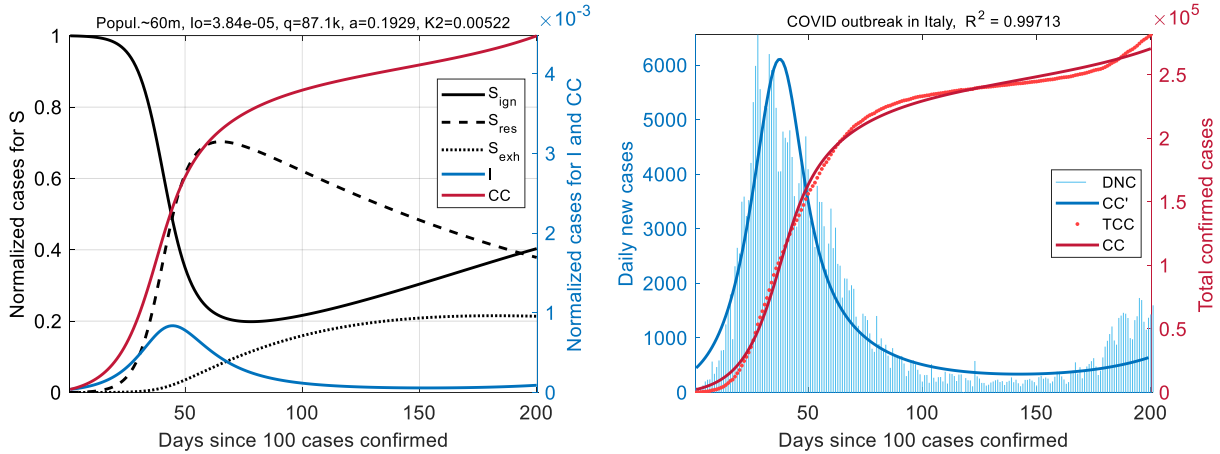


Fig. 1 Coronavirus outbreak in China. The dynamics of the SIR_{SS} model is shown at the **top**: S_{ign} , S_{res} , S_{exh} , I , and $CC = I + R$. Fitted COVID data in absolute values (TCC and DNC) is displayed at the **bottom**.

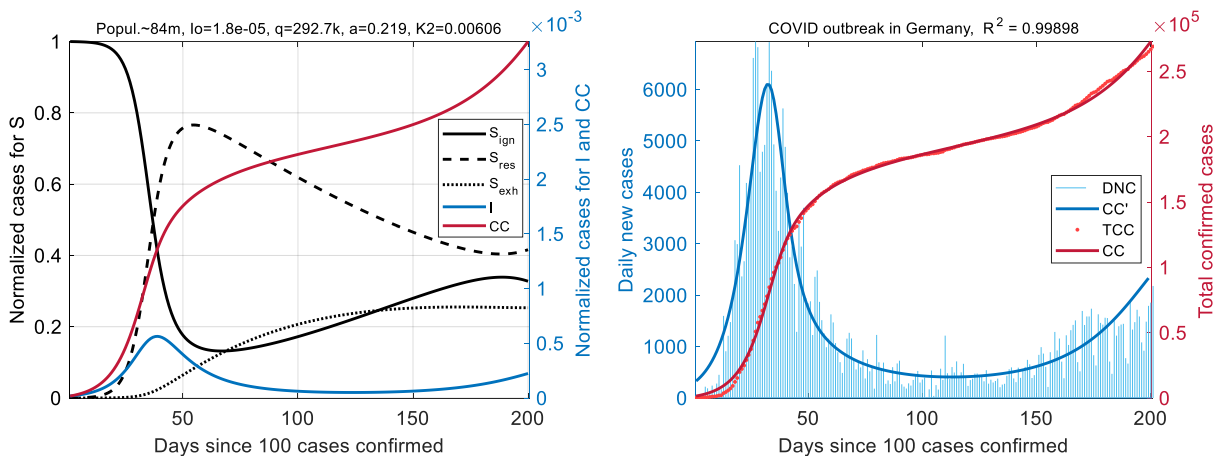
The beginning of the infection spread is characterized by single wave, followed by a plateau on $CC(t)$. Fractions S_{ign} and S_{res} quickly interchange with an increase in $I(t)$, S_{exh} gradually increases to a relatively low level of ~15%.

The first COVID-19 outbreaks in Europe. The general sample of 12 countries was divided into 4 groups of three items each. First, we looked at the large European countries, where the coronavirus outbreak occurred at the beginning of the pandemic: Italy, Germany, and United Kingdom (Fig. 2). An interval of 200 days was also chosen for the simulations.

Italy



Germany



United Kingdom

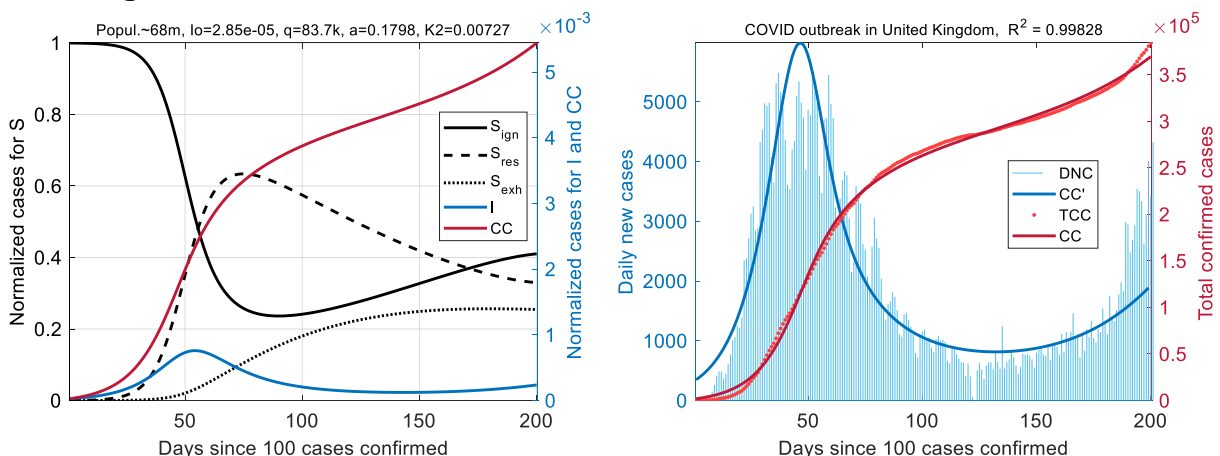
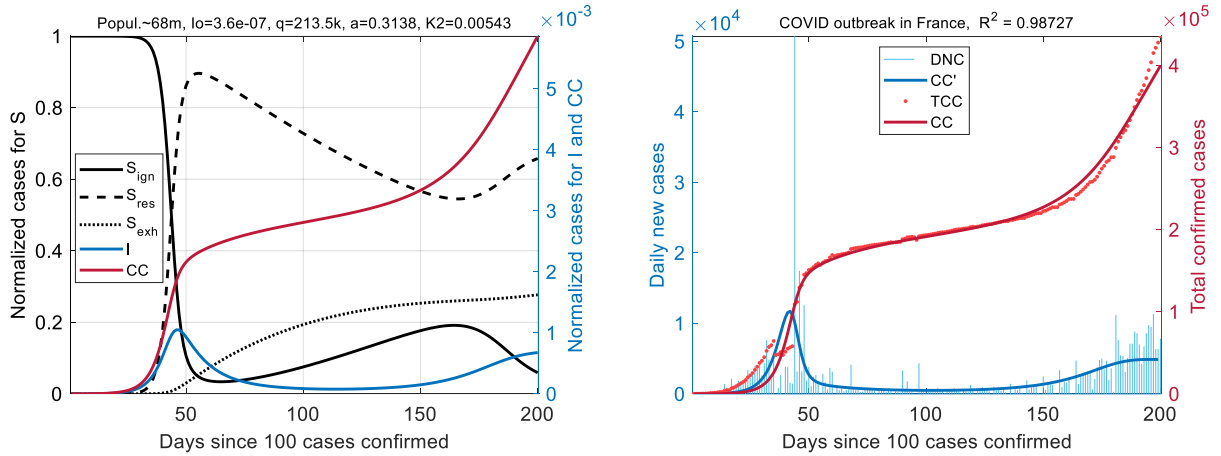


Fig. 2 Earliest coronavirus outbreaks in Europe. Results for Italy (top panel), Germany (center), and United Kingdom (bottom). The dynamics of the epidemic spread are similar and are characterized by a profile containing the full first wave and the beginning of the second wave.

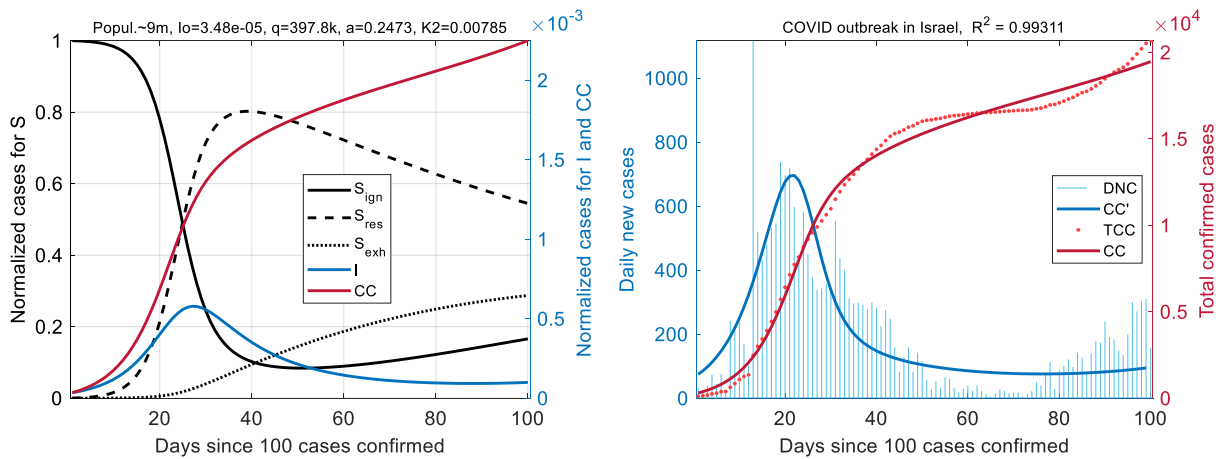
The results demonstrate almost complete match of total cumulative (TCC) and daily new cases (DNC) for the SIR_{ss} model data and the COVID statistics ($R^2 > 0.997$). Note that the dynamics of the epidemic spread was accompanied by mutual oscillations of $S_{\text{ign}}(t)$ and $S_{\text{res}}(t)$ with sustained leakage into the exhausted fraction $S_{\text{exh}}(t)$. The number of S_{exh} reaches saturation level after the end of the first epidemic wave. Curves for infected state, $I(t)$ and $\text{DNC}(t) = \text{TCC}'(t)$, show the two-wave dynamics. The SIR_{ss} model demonstrates the effect of reduction in morbidity at the peak of the first wave due to the rapid stress response on the increase of the infected cases and, hence, the increase in the resistant fraction $S_{\text{res}}(t)$. Consequently, the $I(t)$ dependence enters the second wave due to the accumulation of social stress and exhaustion caused by restrictions. This distinguishes our SIR_{ss} model from the classical SIR, characterized by the depletion of potential carriers of the infection right after the first wave. Thereafter cumulative number of cases (CC) reaches the stationary level. For example, in the simplest SIR model with two parameters (a, b), only one epidemic wave $I(t)$ can exist. Function $\text{CC}(t) = I(t) + R(t)$ is a sigmoid with a saturation level of 32% of the population at parameters (0.12, 0.1) and 80% of the population at (0.2, 0.1). Observations show that the exponential growth of $I(t)$ cannot last for too long, while the total pandemic coverage cannot reach dozens of percent of the population on such time scales.

Countries with a high resistance index. Next, we analyzed the infection data of COVID-19 for countries where the coronavirus outbreak evolved dramatically like in China: it was relatively short-lived, and after it, the morbidity rate $\text{DNC}(t)$ rapidly dropped to a low level. For this purpose data about France, Israel, and Spain were selected and analyzed (**Fig. 3**). Several trends were revealed from the results in **Table 1**. The parameter q , which is responsible for the mobilization response, for France and Israel is several times higher than the median value $q^* = 85.2$. At the same time, in France and Spain, the infection rate, a , takes on abnormally high values: 0.3138 and 0.3770 relative to the median, $a^* = 0.2065$. Thus, the tendency of society to trigger into the *alarm* state, combined with a high infection rate, leads to highly correlated society's response²³. Note, that at the peak the fraction of actively resistant people S_{res} can rise up to 90% of total population.

France



Israel



Spain

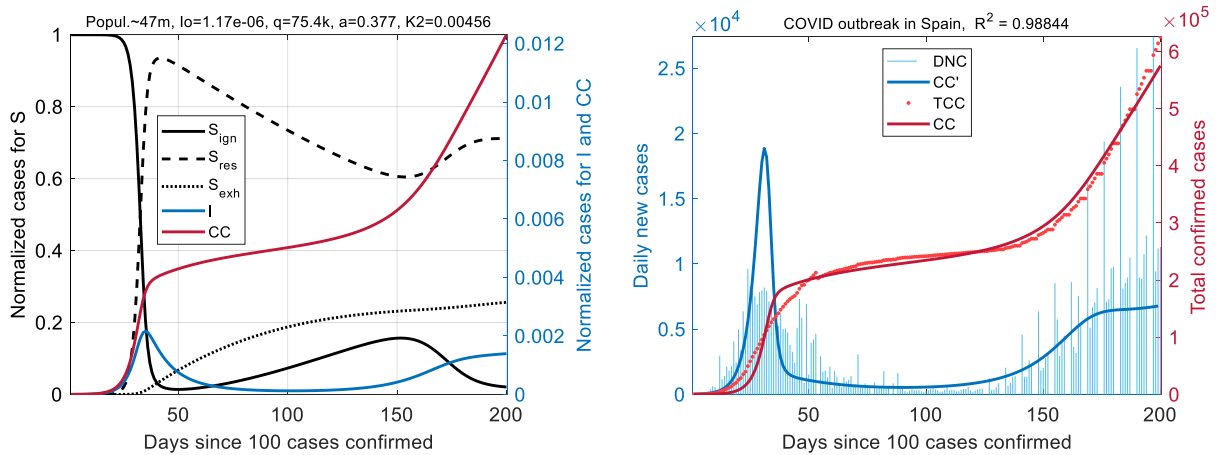


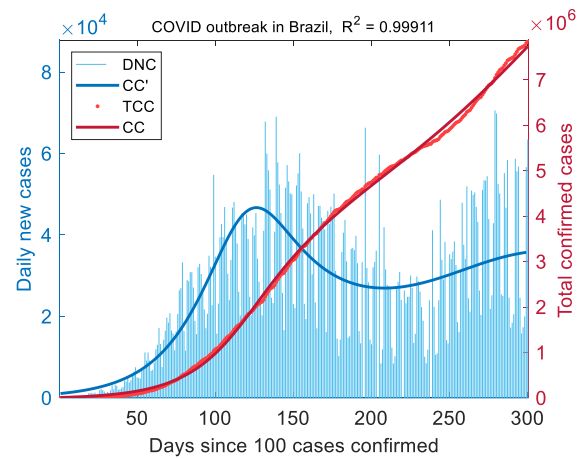
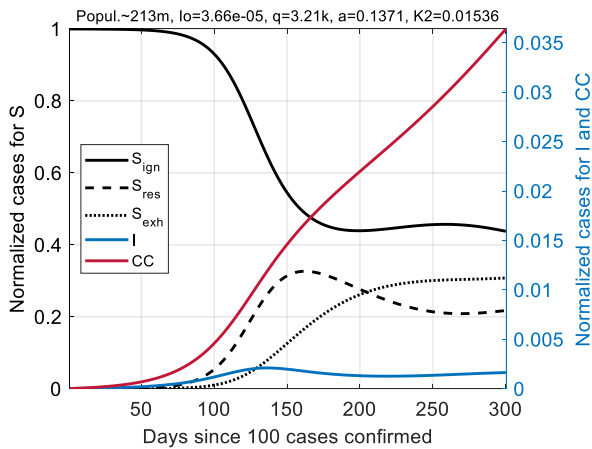
Fig. 3 Coronavirus outbreaks in countries with a high resistance index. Results for France (top panel), Israel (center), and Spain (bottom). The outbreaks dynamics are characterized by a rapid increase in the S_{res} fraction during the peak of the first wave and the formation of protracted plateau on $CC(t)$ with low DNC indices. To simulate the spread of COVID in Israel (population is less than 10 million), we take an interval of 100 days. Numerous data corrections in France and Spain for the period April'20-May'20 lead to negligible discrepancies between the CC and TCC profiles.

Countries with a low resistance index. On the contrary, when the parameter q takes small values, the behavioral reaction of the population to the $I(t)$ growth is weakly expressed. This case corresponds to the third group of countries selected for analysis: Brazil, India, and Russia (**Fig. 4**). At $q \ll q^*$, the similarity of our SIRss model with the classical one is high. Combined with the low infection rate, it leads to the "lengthening" of the first epidemic wave in the time line. The fraction of resistant population, $S_{\text{res}}(t)$, over the entire interval of the outbreak is less than 40%.

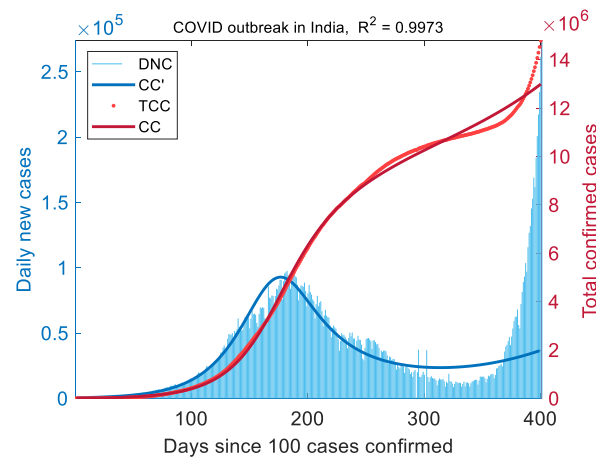
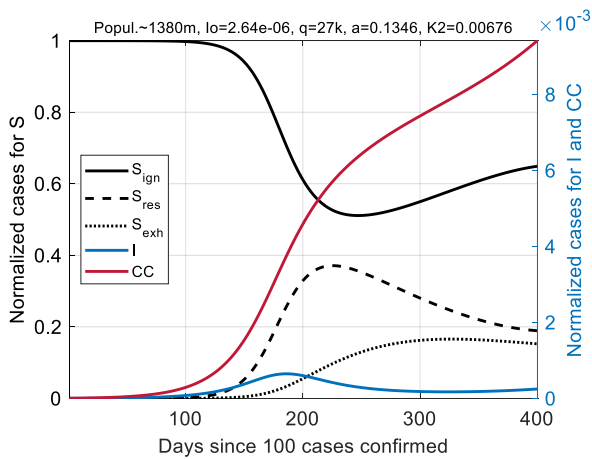
The K_2 parameter for India, which determines the predisposition to trigger into exhaustion mode, along with all 5 European countries analyzed, forms the top-6 lowest exhaustion rates in general sample, while it was only lower than the parameter for the UK. Nevertheless, in India this did not prevent $S_{\text{exh}}(t)$ from evolving at the lowest level among countries of general sample, not exceeding 20%, due to the constantly low level in fraction S_{res} . This parameter for Russia (13.45×10^{-3}) and Brazil (15.36×10^{-3}) was significantly higher than the median $K_2^* = 7.27 \times 10^{-3}$, however, the saturation level $S_{\text{exh}}^* \sim 30\%$, which was comparable to Western European countries with minimal K_2 .

Note, that distinctive feature of this group was the lower morbidity rate a , which was in the top-3 of the lowest values of a . It required much longer time intervals for simulation (up to 400 days). The persistence of high fraction S_{ign} , in contrast to the countries of the second group, can be a precondition for the imminent emergence of the second, more substantial epidemic wave without the rest period, characterized by the $\text{DNC}(t)$ profile with a low plateau (**Fig. 3**). One can notice this fact in the official COVID-19 statistics.

Brazil



India



Russia

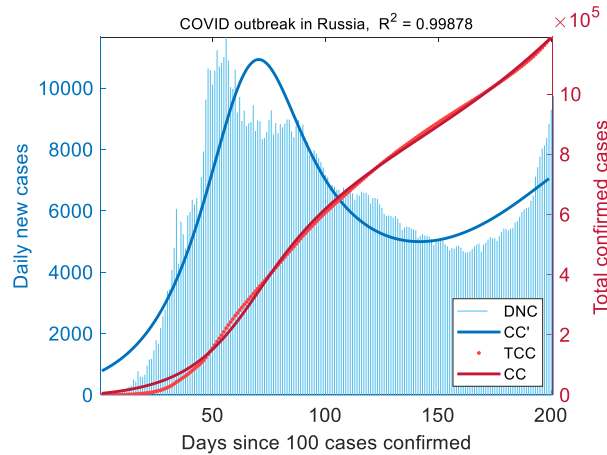
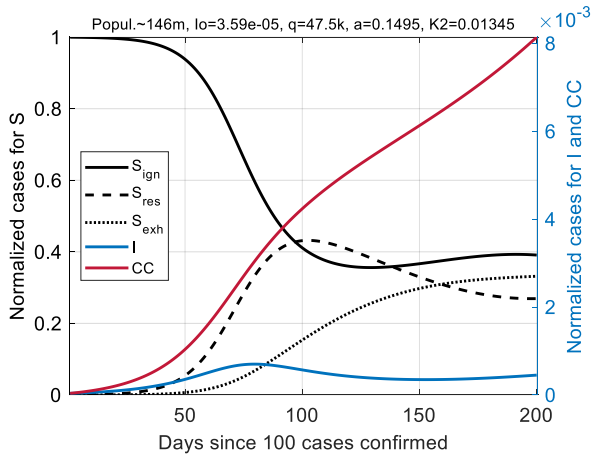
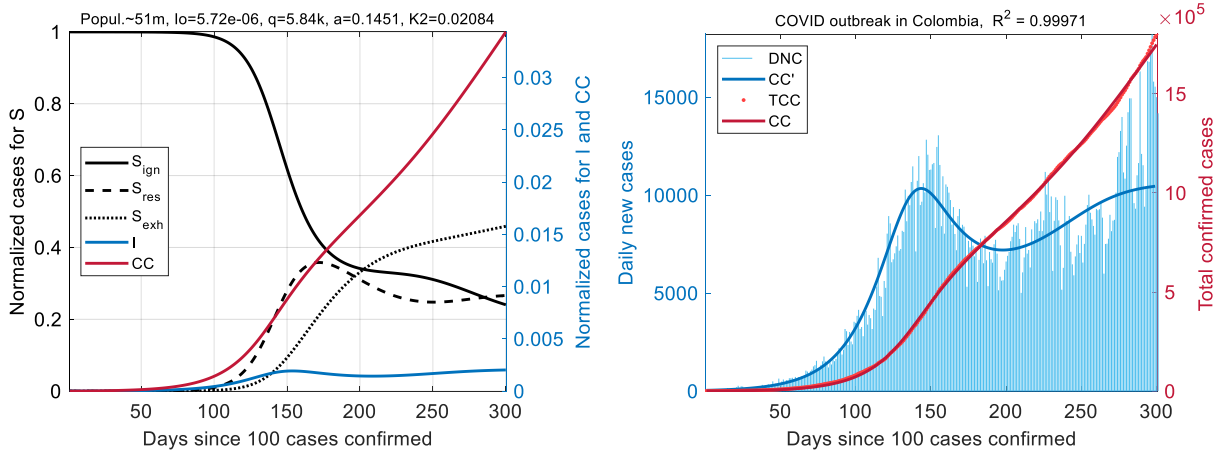


Fig. 4 Coronavirus outbreaks in countries with a low resistance index. Results for Brazil (top panel), India (center), and Russia (bottom). The dynamics profiles are characterized by a low S_{res} and a high S_{ign} in comparison with the previous groups. The exhausted fraction of the population S_{exh} , on the contrary, is quantitatively comparable and evolves in approximately the same scenario. The end of the first wave $I(t)$ smoothly turns into the second one. To simulate the spread of COVID in Brazil and India, which have large populations, intervals of 300 and 400 days were taken, respectively.

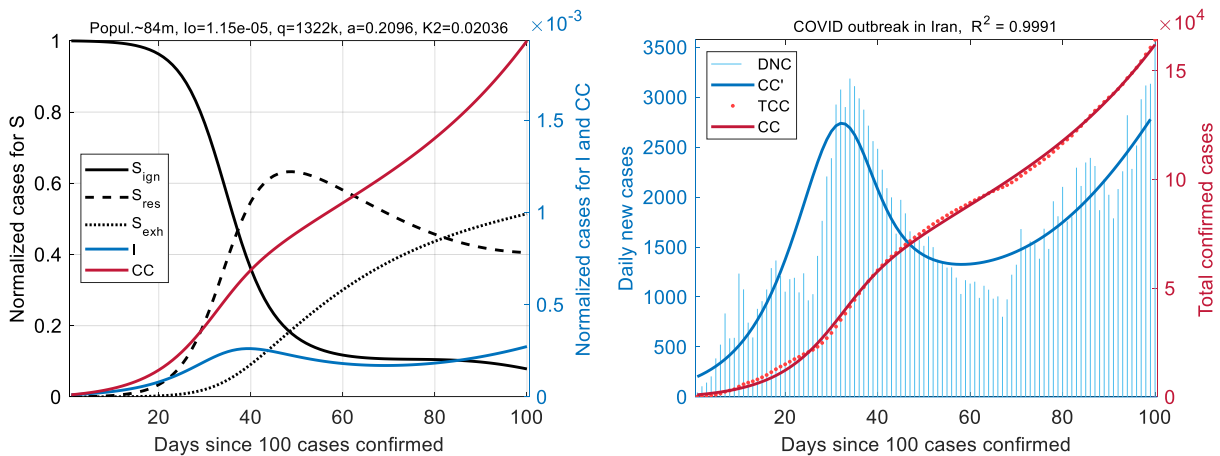
Countries with a high exhaustion rate. Next, we analyzed COVID data for the remaining three countries: Colombia, Iran, and USA (**Fig. 5**). This group was characterized by relatively high values of the exhausted population, $S_{exh} \sim 50\%$. As expected, the parameter $K_2 \sim 20 \times 10^{-3}$ took extremely high values; this group is in the top-3 countries from the general sample in terms of the K_2 coefficient. Ordinary, infection rates $a \sim 0.15-0.2$ indicated the average growth rate of the cumulative cases number. Large scatter of values of q illustrated the weak dependence of $CC(t)$ profile on this parameter.

Similarly to the previous group formation of the second epidemic wave was also revealed. However, in this case, the forecast foreshadows crucially "huge" wave, according to which the DNC values may be many times greater than the first peak.

Colombia



Iran



United States

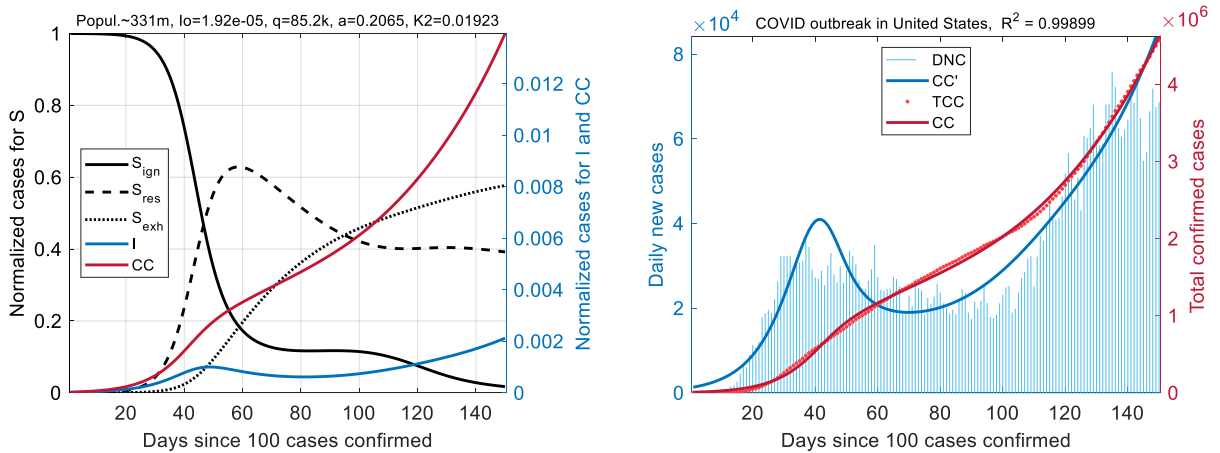


Fig. 5 Coronavirus outbreaks in countries with extremely high exhaustion rate. Results for Colombia (top panel), Iran (center), and United States (bottom). The main trend here is the rapid accumulation of exhausted people S_{exh} (up to ~50% over a period of 50-150 days, if taken from the peak of the first wave). At the same time, the S_{ign} fraction can remain quite small. The first wave of $I(t)$ rapidly turns into the second one without a significant decline relative to the peak values. The time intervals for the simulations were chosen empirically.

Discussion

We demonstrated how the dynamics of the COVID-19 epidemics is mainly driven by the dynamics of social stress. The large difference between epidemics in different countries is caused by social differences and not by real epidemiological (biological) factors, at least until new local viral mutations appear.

The simple SIR_{ss} model works well for 200-300 days of pandemics. We cannot expect that such a simple model will work much longer because various reasons. It has limitations and does not take into account many factors that arise during epidemics, for example:

- Improvement of medical and biological protection methods like new medicine and vaccination;
- Changing government decisions affecting the behavior of millions of people;
- Economic trends;
- Viral mutations.

All these changes require modification of the coefficients of the model and, more importantly, entail the introduction of more processes, such as dynamics of attitudes towards vaccination, social conflicts, and changes in economics.

It may seem rather surprising that the simple SIR_{ss} model, which hardly claims to account for all the epidemiological details of COVID-19, was flexible enough to describe the response of society to virus intervention and subsequent adaptation. At the scale of countries the model was sufficient to describe different kind of statistics of available data with high accuracy.

Even more important than making predictions, our model allows us to assess the development of the epidemic and strategies to combat it for countries with different social structures and cultural traditions. The difference between countries is very clearly represented in kinetic constants.

The model parameters were fitted to various empirical data using a global optimization algorithm (a kind of machine learning). The parameters of social stress response in different countries were estimated. Two of them vary significantly between countries and characterize them:

K_2 (exhaustion rate or the inverse time of exhaustion) and q (stress response or mobilization rate).

The results (**Table 1**) can be summarized as follows.

- A very low K_2 value combined with an extremely high q allows countries to avoid a second wave and remain with the classic single peak profile in the dynamics of the infected fraction, $I(t)$.
- A very high K_2 will inevitably lead to a double-peaked wave, where the second can be particularly large.
- A low K_2 value, together with a high q and a high a (morbidity), provokes two split waves at $I(t)$ with a protracted plateau at $CC(t)$.

The choice of the simplest model of epidemics driven by social stress was almost unambiguous. Further development has many more versions. There are many questions about immunity, the evolution of viruses, the dynamics of opinion, the logic of government decisions, the feedback from social stress to governments, the dynamics of the economy during pandemics, and many others. Each complex model will have many parameters to fit to the data, and the reliability of each value may be questioned. However, we believe that when sufficient data is available, an extended model will be formulated and fitted. The key issue is the combination of modeling social processes with the dynamics of immunity, viral evolution and economics.

Such models will provide us with tools to quantify different situations, evaluate solutions, and play out different “*in silico*” scenarios to develop anti-epidemic strategies specific to a particular society: country, region, or social group.

Methods

SIR_{ss} model features description. SIR-type models basically describe two following types of transitions: $S + I \rightarrow 2I$ and $I \rightarrow R$. The first one defines close contact infection of a susceptible person with an infected person; the second one describes the relaxation process of recovery or death from the disease. In state R , a person is no longer contagious and does not return back to state S ,

therefore, for relatively short periods of time (for example, no more than a year), one can take total population as constant: $S(t) + I(t) + R(t) = 1$.

However, basic SIR models do not take into account the permanent presence of a person in the information field and his reaction to events taking place in society. Significant administrative decisions, which in most cases come down to tightening hygiene standards and social distancing, lead to a natural response of the living human organisms.

We introduce an enhancement of the SIR model that takes into account the impact of social stress factor⁷. According to the general adaptation syndrome (GAS) theory, there are three chronological stages of the stress response: *alarm*, *resistance*, and *exhaustion*. Given the fraction of the population not under stress and neglecting the alarm stage, we assume that susceptible individuals (S) may have three types of behavior: *ignorant* or unaware of the epidemic (S_{ign}), rationally *resistant* (S_{res}), and *exhausted* (S_{exh}) that do not react on the external stimuli (this is a sort of refractory period). In other words: $S(t) = S_{ign}(t) + S_{res}(t) + S_{exh}(t)$.

In accordance with this add-on, three additional probabilistic transitions caused by social stress factor emerge in the detailed SIR_{ss} model:

- 1) $S_{ign} + 2I \rightarrow S_{res} + 2I$ – mobilization reaction (fast), the probability is proportional to the square of the infected fraction at the moment $I(t)$ to capture a super-linear increase in alarm reaction to an increase in the number of infected people;
- 2) $S_{res} \rightarrow S_{exh}$ – steady exhaustion due to COVID-19 restrictions (slow);
- 3) $S_{exh} \rightarrow S_{ign}$ – transition to the ignoring state (slow).

The first transition represents the stress response on the steadily increasing fraction of the infected population. The second transition describes a relaxation of the resistant fraction into the category of exhausted ones. The third transition completes the loop within the S state and reflects the slow leak of the exhausted people to the state of ignoring the epidemic.

The infection rates of S_{exh} and S_{ign} are the same as in the basic SIR model. For fraction S_{res} , probability of transition to I is significantly lower, and in the limit case one can take this category as not susceptible to disease at all.

Diff. equations and discrete time model. According to the above mentioned transitions the SIR_{SS} model has five variables, $S_{ign}(t)$, $S_{res}(t)$, $S_{exh}(t)$, $I(t)$, $R(t)$, and can be formulated as follows:

$$\frac{dS_{ign}}{dt} = -qS_{ign}I^2 - aS_{ign}I + K_3S_{exh} \quad (1)$$

$$\frac{dS_{res}}{dt} = qS_{ign}I^2 - K_2S_{res} \quad (2)$$

$$\frac{dS_{exh}}{dt} = -aS_{exh}I + K_2S_{res} - K_3S_{exh} \quad (3)$$

$$\frac{dI}{dt} = aS_{exh}I + aS_{ign}I - bI \quad (4)$$

$$\frac{dR}{dt} = bI \quad (5)$$

where parameter $K_1 = q$ is the rate of transition to the resistant state mediated by a stress response in society, K_2 is the exhaustion rate due to restrictions ($K_2 \ll 1$), K_3 is the constant of transition to a state of ignorance ($K_3 \ll 1$), $K_4 = a$ is the morbidity rate, $K_5 = b$ is the recovery constant.

The following constants were used in the work: $b = 0.1$, $K_3 = 0.01$. Parameters a , K_2 and q are selected for various countries to best match the observed data on the COVID-19 outbreak. The initial fraction of infected population $I(t=0) = I_0 \ll 1$ is also taken as a variable parameter. The rest of the population is assigned ignorant by default: $S_{ign} = 1 - I_0 \approx 1$.

The choice of parameters b and K_3 as constants is determined by the following considerations. The dynamics of the outbreak onset (when $S_{res} \approx S_{exh} \approx 0$) depends on the ratio of a and b . On a large time scale, the profile of the epidemic spread depends on the relationship between K_2 and K_3 . Thus, we choose b and K_3 as the references for a and K_2 , respectively. Trial simulations showed that the correspondence between the model and the infection data of COVID-19 at other values of b and K_3 is provided at the same top level. This fact confirms our choice.

Since retrospective data on COVID-19 is provided with a sampling of one day, all computations were performed with the said time interval or with an interval of an integer number of times less ($dt = 1, 0.5, 0.1, 0.02$, etc.). Equations (1)-(5), were transformed into a discrete-time system using the substitution: $dX/dt = X(t) - X(t-1)$, where X is alternately replaced by the variables of the proposed SIR_{SS} model, $t \in \mathbb{N}$.

Comparison with COVID-19 observations. Cumulative confirmed COVID-19 cases and daily new cases were obtained from a public source of statistical information: the COVID-19 Data Repository by the Center for Systems Science and Engineering (CSSE) at Johns Hopkins University (JHU). Computation of phase variables dynamics from equations (1)-(5) was carried out using custom-made MatLab software. To assess the relevance of the main result reproduced by the model – the dependence of the number of cumulative cases on time: $CC(t) = I(t) + R(t)$ – the coefficient of determination R^2 was calculated. As the starting point for the algorithm to work ($t = 0$), we choose the day since at least 100 cases of COVID-19 were confirmed. The time interval for comparing the two samples was equal to the number of days of the modeled trace of $CC(t)$. The search for the global maximum of the R^2 was implemented in the parameter space (a, K_2, q, I_0) , at which the model reproduces epidemics dynamics that is closest to the observed one.

Data availability

The series of COVID-19 confirmed cases for all countries of the world are publicly available at data repository of *Our World in Data* project: <https://github.com/owid/covid-19-data/tree/master/public/data> (direct link to Excel file: <https://covid.ourworldindata.org/data/owid-covid-data.xlsx>). Raw data come from the COVID-19 Data Repository by the Center for Systems Science and Engineering (CSSE) at Johns Hopkins University (JHU) at <https://github.com/CSSEGISandData/COVID-19>.

Code availability

Code used to produce the results presented herein is available in a public GitHub repository at <https://github.com/forester52/COVID-19-outbreak-model>.

References

1. Dehning, J. et al. Inferring change points in the spread of COVID-19 reveals the effectiveness of interventions. *Science* **369**, 1-11 (2020).
2. Chang, S. et al. Mobility network models of COVID-19 explain inequities and inform reopening. *Nature* **589**, 82-87 (2021).
3. Huang, J., & Qi, G. Effects of control measures on the dynamics of COVID-19 and double-peak behavior in Spain. *Nonlinear Dyn.* **101**, 1889-1899 (2020).
4. Liu, X., Zheng, X., & Balachandran, B. COVID-19: data-driven dynamics, statistical and distributed delay models, and observations. *Nonlinear Dyn.* **101**, 1527-1543 (2020).
5. Young, L. S., Ruschel, S., Yanchuk, S., & Pereira, T. Consequences of delays and imperfect implementation of isolation in epidemic control. *Sci. Rep.* **9**, 1-9 (2019).
6. Lux, T. The social dynamics of COVID-19. *Physica A* **567**, 125710 (2021).
7. Selye, H. The general adaptation syndrome and the diseases of adaptation. *J. Clin. Endocrinol.* **6**, 117-230 (1946).
8. Galam, S. *Sociophysics: A Physicist's Modeling of Psycho-political Phenomena*, Springer, Boston, MA (2012).
9. Tang, B. et al. Estimation of the transmission risk of the 2019-nCoV and its implication for public health interventions. *J. Clin. Med.* **9**, 462 (2020).
10. Wu, J. T., Leung, K., & Leung, G. M. Nowcasting and forecasting the potential domestic and international spread of the 2019-nCoV outbreak originating in Wuhan, China: a modelling study. *Lancet* **395**, 689-697 (2020).

11. Cooke, K. L., & Van Den Driessche, P. Analysis of an SEIRS epidemic model with two delays. *J. Math. Biol.* **35**, 240-260 (1996).
12. Wang, W. Global behavior of an SEIRS epidemic model with time delays. *Appl. Math. Lett.* **15**, 423-428 (2002).
13. Chen, Y. C., Lu, P. E., Chang, C. S., & Liu, T. H. A time-dependent SIR model for COVID-19 with undetectable infected persons. *IEEE Trans. Network Sci. Eng.* **7**, 3279-3294 (2020).
14. Cooper, I., Mondal, A., & Antonopoulos, C. G. A SIR model assumption for the spread of COVID-19 in different communities. *Chaos, Solitons Fractals* **139**, 110057 (2020).
15. Oliveira, J. F. et al. Mathematical modeling of COVID-19 in 14.8 million individuals in Bahia, Brazil. *Nat. Commun.* **12**, 1-13 (2021).
16. Liu, C., Wu, X., Niu, R., Wu, X., & Fan, R. A new SAIR model on complex networks for analysing the 2019 novel coronavirus (COVID-19). *Nonlinear Dyn.* **101**, 1777-1787 (2020).
17. Rong, X., Yang, L., Chu, H., & Fan, M. Effect of delay in diagnosis on transmission of COVID-19. *Math. Biosci. Eng.* **17**, 2725-2740 (2020).
18. Cinelli, M. et al. The COVID-19 social media infodemic. *Sci. Rep.* **10**, 1-10 (2020).
19. Selye, H. A syndrome produced by diverse nocuous agents. *Nature* **138**, 32 (1936)
20. Cannon, W. B. *Bodily Changes in Pain, Hunger, Fear and Rage: an Account of Recent Researches into the Function of Emotional Excitement*, D Appleton & Company, New York and London (1915).
21. Selye, H. *The Stress of Life*, McGraw-Hill, New York, NY (1956).
22. Hinkle Jr, L. E. The concept of “stress” in the biological and social sciences. *Sci. Med. Man* **1**, 31-48 (1973).
23. Gorban, A. N., Tyukina, T. A., Pokidysheva, L. I., Smirnov, E. V. Dynamic and thermodynamic models of adaptation. *Phys. Life Rev.* **37**, 17–64 (2021).

Acknowledgements

The reported study was funded by RFBR according to the research project No. 20-04-60078.

Author contributions

I.A.K. – design of model experiments, model simulation, data analysis, results interpretation, writing the manuscript. E.V.P. – model simulation, writing the manuscript. V.B.K. – model simulation, results interpretation, writing the manuscript. E.M.M. – model formulation. A.N.G. – model formulation, results interpretation, writing the manuscript.

Competing interests

The authors declare no competing interests.

Additional information

Correspondence and requests for materials should be addressed to I.A.K.